Tellus (1999), 51A, 552–573
Printed in UK. All rights reserved

TELLUS
ISSN 0280–6495

Breaking Rossby waves in the barotropic atmosphere with parameterized baroclinic instability

By H. L. TANAKA[1]* and YASUSHI WATARAI[2], [1]*Institute of Geoscience, University of Tsukuba, Tsukuba, 305-8571 Japan;* [2]*Doctoral Program in Geoscience, University of Tsukuba, Tsukuba, 305-8571 Japan*

(Manuscript received 24 September 1998; in final form 9 June 1999)

ABSTRACT

In this study, we conducted a series of numerical experiments of breaking Rossby waves in the barotropic atmosphere using a simple barotropic model which implements parametrization of baroclinic instability. Exponential growth of unstable modes must terminate eventually when the waves become finite amplitude. The non-linear evolution of amplified Rossby waves is examined by analyzing the potential vorticity (PV) field in order to assess the criterion of the Rossby wave breaking in a barotropic model atmosphere. For a control run of the wave-6 experiment, growing unstable wavenumber $n = 6$ is saturated when the wave energy attains approximately 20% of zonal energy of the basic flow. The energy supply at $n = 6$ is balanced with energy transfer to zonal flow and to its harmonics of $n = 12$ and 18 by weak non-linear interactions, maintaining a steady configuration of a surf zone structure. The existence of the negative meridional gradient of PV is the necessary condition for the wave saturation. We then attempted to break the waves intentionally by increasing the growth rate of the unstable mode. It is found that the regularity of Rossby wave progression is lost and the overturning of high and low PV centers occurs when the growth rate is increased by 30%. Associated with the Rossby wave breaking, not only the harmonic waves but all zonal waves are amplified by the fully non-linear interactions among all waves. It is demonstrated that the transition from the weakly non-linear regime to fully non-linear regime in the energy transfer is the key factor for the Rossby wave breaking so that the supplied energy is effectively dissipated by all waves.

1. Introduction

Rossby wave breaking (or planetary wave breaking) has long been studied extensively, especially in middle atmosphere in relation to stratospheric sudden warming. A wave–mean flow interaction associated with the stratospheric sudden warming is a realization of Rossby wave breaking, where amplified planetary waves ultimately break down to deposit the easterly momentum into the mean flow. The dynamical stability of robust polar vortex draws great attention in relation to a study of ozone hole in the Southern Hemisphere (Juckes and McIntyre, 1987; Juckes, 1989). Intrusion of a tongue of low potential vorticity (PV) into the Arctic results in an enhanced material mixing in and outside the polar vortex which prevent the extreme low temperature in the Northern Hemisphere. Such a material mixing is another realization of Rossby wave breaking.

In the troposphere the Rossby wave breaking has been studied in the context of non-linear life cycle of baroclinic waves (Simmons and Hoskins, 1976; Throncroft et al., 1993; Whitaker and Snyder, 1993; Govindasamy and Garner, 1997; Balasubramanian and Garner, 1997; Hartmann and Zuercher, 1998). The detailed studies of the

* Corresponding author.

life cycle are conducted in response to latent heat release, spherical geometry, and barotropic shear, among others. Recently, the Rossby wave breaking draws more attention in conjunction with the onset of blocking in the troposphere. According to a model simulation of blocking by Tanaka (1998), a breaking Rossby wave leads to the onset of blocking, and the blocking itself causes subsequent breakdown of travelling Rossby waves. In that model, travelling Rossby waves grow exponentially by means of parameterized baroclinic instability, so the waves must break down somewhere. A Rossby wave, which grows critical in amplitude, breaks down at a topographically induced stationary ridge and is captured by the stationary ridge. Then, overturning of high and low PV centers takes place there to create a blocking.

An example of blocking formation triggered by a breaking Rossby wave is illustrated in Fig. 1. In the figure, contours of shallow water PV are plotted with latitude in the ordinate and longitude in the abscissa in descending order, respectively, in order to mimic the progression and breaking of waves in analogy of shallow water system at the shore. The high PV in the polar region is hatched to illustrate the breaking waves at the surf zone. The elongation of trough and ridge axes from northwest to southeast and the anti-clockwise overturning of the vortex pair are the major characteristics of Rossby wave breaking induced by baroclinic instability. Fig. 2 illustrates longitude–time section of potential vorticity along 58°N for a life-cycle of a blocking in the barotropic model atmosphere in Tanaka (1998). In the model atmosphere, topographic forcing produces stationary ridges along the west coast of the major continents. A progressively travelling Rossby wave is captured by the topographic ridge and breaks down there to create a blocking. Subsequent Rossby waves are then blocked by the blocking. The decelerated waves exhibit meridional stretch in PV field upstream of the blocking and eventually break down to deposit the fresh low PV into the main body of blocking and high PV into the cut-off low south of it to maintain the blocking system (Shutts, 1983; Tanaka, 1998). In this blocking theory, the Rossby wave breaking appears to play the key role both for the onset and maintenance of blocking. Therefore, it is important to understand the mechanism and criterion of the Rossby wave breaking in more detail for the study and prediction of blocking formation.

Rossby wave breaking was discussed as an analogy of gravity wave breaking by many authors (McIntyre and Palmer, 1983, 1984, 1985; Leovy et al., 1985; Robinson, 1988; Garcia, 1991). The non-linear behavior of overturning waves near the critical layer was analytically investigated by Warn and Warn (1978). Fig. 3 schematically compares gravity wave breaking in the vertical section and Rossby wave breaking in the meridional section. When the isentropic surface overturns wrapping up the contours, negative vertical gradient of potential temperature appears as indicated in the figure. The convective instability is the principal mechanism for gravity wave breaking which eliminate the instability through the convective mixing (Fritts, 1984). Once the gravity waves become convectively unstable, they will be dissipated at a

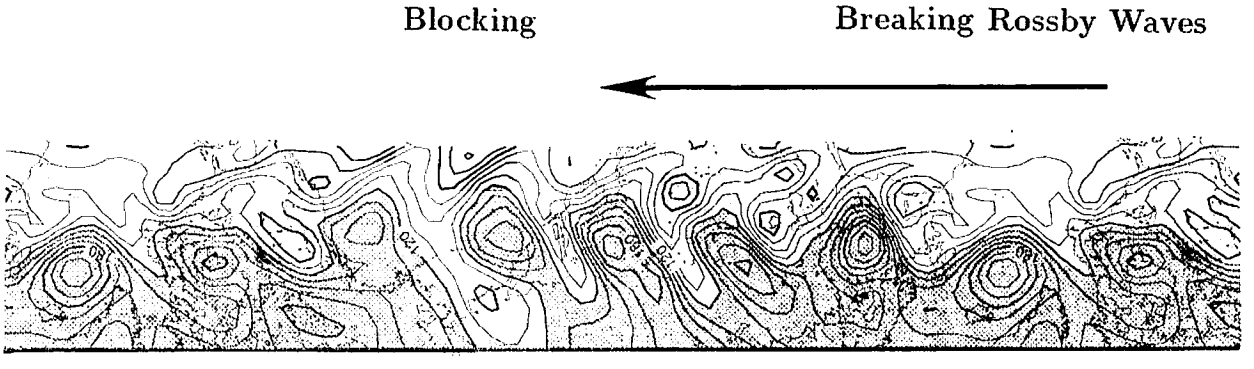

Fig. 1. A blocking formation triggered by breaking Rossby waves, redrafted from the distribution of potential vorticity (PV) in the barotropic model atmosphere. Ordinate and abscissa are the latitudes (70~20°N) and the longitudes (360~0°E), respectively, in descending order. The contours of PV are in the units $10^{-10}\,m^{-1}\,s^{-1}$. The high PV in polar region exceeding the value of 120 is hatched.

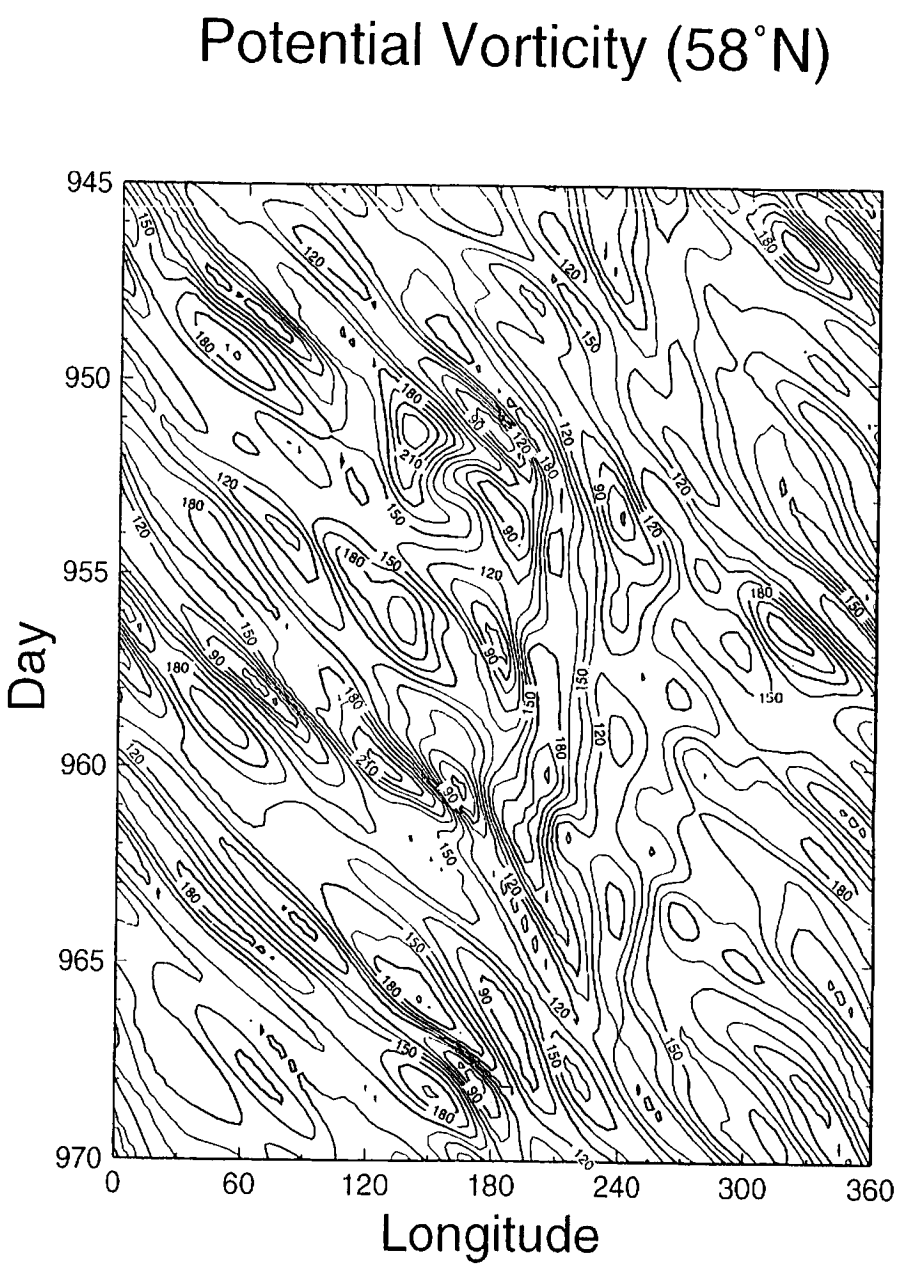

Fig. 2. Longitude–time series of potential vorticity along 58°N for a life-cycle of a blocking in the barotropic model atmosphere. The units are $10^{-10}\,m^{-1}\,s^{-1}$ (after Tanaka, 1998).

rate just sufficient to prevent further amplitude growth. This situation is referred to as wave saturation (Lindzen, 1981). The wave breaking and wave saturation seem to be indistinguishable for gravity wave.

For the Rossby wave, the dynamical analogy is illustrated with potential vorticity contours in the meridional plane. When the high and low PV centers roll up to exhibit surf zone structure, negative meridional gradient of potential vorticity appears as indicated in the figure, this being the necessary condition for barotropic–baroclinic instability of the flow (Charney and Stern, 1962; Haynes, 1989). According to Garcia (1991), the breaking criterion for Rossby wave was defined as the wave amplitude for which the magnitude of the perturbation PV exceeds the background PV. This is a reasonable criterion at which negative meridional gradient of PV appears in the domain.

Although the analogy of Rossby wave breaking is perfectly clear, the theoretical basis of Rossby wave breaking is not well established. For instance, laboratory and field observations indicate that

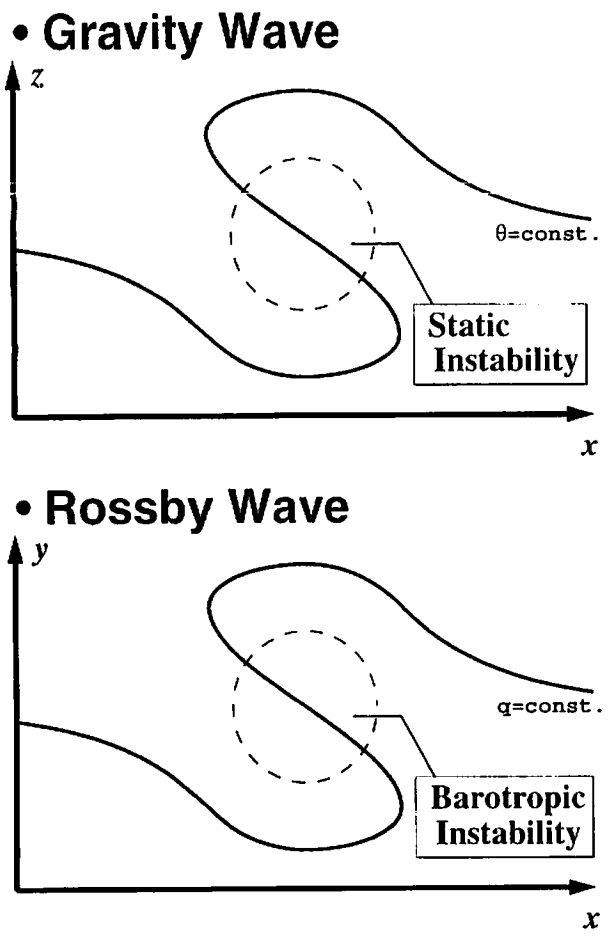

Fig. 3. Schematic illustration of gravity wave breaking in the vertical section (upper) and Rossby wave breaking in the meridional section (lower).

inertial gravity wave breaking leads to the generation of three-dimensional turbulence, whereas the Rossby wave breaking may be treated within the framework of two-dimensional turbulence (McIntyre and Palmer, 1985). The former would produce a number of small eddies, through energy cascade by the gravity wave breaking. The latter, on the other hand, would produce even larger coherent vortices through the inverse energy cascade by the Rossby wave breaking. Namely, synoptic-scale wave breaking may result in excitation of planetary waves. A splitting jet and zonalization are the realization of such a Rossby wave breaking. Two paradigms of cyclonic and anticyclonic evolutions of the vortex pair overturning lead to opposite direction of eddy momentum flux (Thorncroft et al., 1993; Whitaker and Snyder, 1993; Akahori and Yoden, 1996; Govindasamy and Garner, 1997; Balasubramanian and Garner, 1997; Hartmann and Zuercher, 1998). Further study is thus desirable to understand the Rossby wave breaking to confirm if Garcia's analogy is applicable to the study of the blocking onset.

The purpose of this study is to examine the breaking Rossby waves in the barotropic atmosphere using a simple barotropic model which implements parameterization of baroclinic instability. Within the linear framework the parameterized unstable wave with a small amplitude grows exponentially by the baroclinic instability. The exponential growth must, however, terminate at a finite amplitude leading to a wave breaking at certain energy level. We examine the non-linear evolution of the growing Rossby waves and the criterion of the wave breaking in the barotropic atmosphere. The energy flows associated with the Rossby wave breaking are extensively examined in the wavenumber domain.

The paper is organized as follows. In Section 2 model description is presented especially for the detail of the parameterization of baroclinic instability for a barotropic model. The result of experiments are described in Section 3, first for a control run with zonal wavenumber 6. Here, it will be shown that the wave energy is saturated at an approximately constant level, but the wave breaking is not achieved since the surf zone structure is stably maintained in this experiment. For this reason, we attempt to break the wave intentionally by increasing the growth rate of the unstable modes. The results of the breaking Rossby waves and the energetics analysis are discussed in the latter half of Section 3. Concluding remarks are given in Section 4.

2. Model description

2.1. *Primitive equation model*

The model description is detailed in Tanaka (1998), and a brief description is presented here. A system of primitive equations with a spherical coordinate of longitude λ, latitude θ, pressure p, and time t may be reduced to 3 prognostic equations of horizontal motions and thermodynamics for three dependent variables of $U = (u, v, \phi)^{\mathrm{T}}$. Here, u and v are the zonal and meridional components of the horizontal velocity. The variable ϕ is a departure of the local isobaric geopotential from the global mean reference state, and the superscript T denotes a transpose. Using a matrix

notation, these primitive equations may be written as

$$M\frac{\partial U}{\partial t}+LU=N+F. \tag{1}$$

The left-hand side of (1) represents linear terms with matrix operators M and L and the dependent variable vector U. The right-hand side represents a non-linear term vector N and a diabatic term vector F which includes the zonal and meridional components of frictional forces and a diabatic heating rate.

Then, 3-D normal mode functions $\Pi_{nlm}(\lambda, \theta, p)$ are calculated by a tensor product of vertical structure functions (vertical normal modes) and Hough harmonics (horizontal normal modes) which are associated with the linear operators M and L, respectively. It is known that they form a complete set and satisfy an orthonormality condition under a proper inner product. In order to derive a system of spectral primitive equations, we expand the vectors U and F in the 3-D normal mode functions in a resting atmosphere:

$$U(\lambda,\theta,p,t)=\sum_{n=-N}^{N}\sum_{l=0}^{L}\sum_{m=0}^{M}w_{nlm}(t)X_m\Pi_{nlm}(\lambda,\theta,p), \tag{2}$$

$$F(\lambda,\theta,p,t)=\sum_{n=-N}^{N}\sum_{l=0}^{L}\sum_{m=0}^{M}f_{nlm}(t)Y_m\Pi_{nlm}(\lambda,\theta,p). \tag{3}$$

Here the expansion coefficients $w_{nlm}(t)$ and $f_{nlm}(t)$ are the functions of time alone. The subscripts represent zonal wavenumber n, meridional index l, and vertical index m. They are truncated at N, L, and M, respectively. The scaling matrices X_m and Y_m should be defined for each vertical index.

By transforming (1) into a spectral form using the basis of 3-D normal mode functions, we obtain a system of 3-D spectral primitive equations in terms of the spectral expansion coefficients:

$$\frac{dw_i}{d\tau}+i\sigma_i w_i=-i\sum_{jk}r_{ijk}w_jw_k+f_i, \qquad i=1,2,3,\ldots, \tag{4}$$

where τ is a dimensionless time, the symbol σ_i denotes the eigenfrequency of the normal mode at a resting atmosphere, and r_{ijk} is the interaction coefficient for non-linear wave–wave interactions. For simplicity, the triple subscripts nlm are shortened to i.

The spectral primitive eq. (4) was integrated by Tanaka (1995) for the study of a life-cycle of non-linear baroclinic waves. The result clearly shows that baroclinic waves draw energy from baroclinic components of the atmosphere and feed the energy to the barotropic components. It was found that the important baroclinic–barotropic interactions are accomplished by baroclinic instability, which transfers the zonal baroclinic energy to barotropic components of the atmosphere.

2.2. *Eigenvalue problem for linear instability*

The process of baroclinic instability may be readily analyzed by linearizing (4) with respect to a proper zonal basic state. In order to solve the most unstable linear mode, a perturbation method is introduced using notations $\bar{w}_i$ for a time-independent zonal basic state and w' for small perturbations superimposed on the basic states (the same symbols with the original variables are used for convenience). The equation for the first-order term of perturbations becomes

$$\frac{dw_i}{d\tau}+i\sigma_i w_i=-i\sum_{j=1}^{K}\left(\sum_{k=1}^{K}(r_{ijk}+r_{ikj})\bar{w}_k\right)w_j, \qquad i=1,2,3,\ldots, \tag{5}$$

where the index k is used for the basic state and i and j for the perturbations. Here, inviscid and adiabatic eddy is examined, disregarding the forcing for perturbations. For a zonal basic state ($\bar{w}_k\neq 0$ if $n=0$), we can rewrite the equation in terms of a matrix form for each $n\geqslant 0$:

$$\frac{d}{d\tau}W_n+iD_nW_n=-iB_nW_n, \qquad n=1,2,\ldots,N, \tag{6}$$

where

$$W_n=(w_1,\ldots,w_i,\ldots,w_K)^{\mathrm{T}}, \tag{7}$$

$$D=\mathrm{diag}(\sigma_1,\ldots,\sigma_i,\ldots,\sigma_K), \tag{8}$$

and $K=(L+1)(M+1)$. The (i,j) entries of the matrices B, namely b_{ij}, are evaluated by the expansion coefficients of the basic state $\bar{w}_k$:

$$b_{ij}=\sum_{k=1}^{K}(r_{ijk}+r_{ikj})\bar{w}_k, \qquad i,j=1,2,\ldots,K, \tag{9}$$

The zonal–wave interaction B_n vanishes for a basic state at rest ($\bar{w}_k=0$), thus the eq. (6) satisfies the normal mode relation for Laplace's classical tidal theory.

Because (6) is linear, we can assume the solution of W_n as:

$$W_n(\tau) = \xi \exp(-i\nu\tau). \quad (10)$$

The initial value problem (6) is then reduced to an eigenvalue problem for a real matrix to obtain eigenvectors ξ and eigenvalues ν as:

$$\nu\xi = (D_n + B_n)\xi. \quad (11)$$

Those eigenpairs n and ξ are evaluated by the standard matrix eigenvalue solver. They will be used as the important tools of the parameterization of baroclinic instability for a barotropic model. The distribution of the growth rates and the structure of the unstable modes are discussed by Tanaka and Kung (1989) and Tanaka and Sun (1990) for a basic state of monthly mean FGGE (First GARP Global Experiment) data for January 1979. The growth rate of the most unstable Charney mode is about 0.47 day^{-1} at the zonal wavenumber 7, which corresponds to the e-folding time about 2 days.

2.3. *Modified basic non-linear equation*

We now return to the fully non-linear equation retrieving the wave–wave interactions and external forcing disregarded in (5).

$$\frac{dw_i}{d\tau} + i\sigma_i w_i = -i \sum_{j=1}^{K} \left(\sum_{k=1}^{K} (r_{ijk} + r_{ikj})\bar{w}_k \right) w_j - i \sum_{jk} r_{ijk} w_j w_k + f_i, \qquad i = 1, 2, 3, \ldots, K. \quad (12)$$

The first term in the right-hand side represents linear zonal–wave interactions as appeared in (5), and the second term represents the rest of nonlinear wave–wave interactions. Note that the state variables here are finite-amplitude deviations from the time-independent zonal basic state.

Supposing that the eigenspace for the matrix $(D_n + B_n)$ in (11) is full rank without any multiple roots, we have K linearly independent non-orthogonal eigenvectors ξ_l, $l = 1, 2, 3, \ldots, K$. The state variable w_i may then be expanded in the basis of the eigenvectors ξ_l for each zonal wavenumber:

$$w_i(\tau) = \sum_l a_l(\tau)\xi_{li}, \quad (13)$$

where the amplitude coefficients $a_l(\tau)$ are supposed to be determined by solving a linear system. Since $w_i(\tau)$ is a function of time, so is the amplitude coefficient $a_l(\tau)$. Substituting (13) into the 1st term of the right-hand side of (12), the linear operators associated with the zonal–wave interactions may be reduced to their eigenvalues of ν_l in reference to (11) for each zonal wavenumber:

$$\frac{dw_i}{d\tau} + i\sigma_i w_i = -i \sum_l (\nu_l - \sigma_i) a_l \xi_{li} - i \sum_{jk} r_{ijk} w_j w_k + f_i, \qquad i = 1, 2, 3, \ldots, K, \quad (14)$$

Note that the complicated zonal–wave interactions are represented by the summation of eigenmodes. The real part of eigenvalues are modified by σ_i.

When the model eq. (14) is integrated from infinitesimal white noise of w_i superimposed on the basic state, the most unstable mode $a_1\xi_{1i}$ would soon dominate the other modes, growing exponentially with the growth rate determined by ν_1, as predicted by the linear theory. The barotropic components grow in proportion to baroclinic components maintaining the normal mode structure ξ_{1i}. It is in this process of zonal–wave interactions where the baroclinic energy in the basic state is converted to barotropic energy in eddies. Refer to Tanaka (1995) for the energy flows associated with the baroclinic instability which explains the energy flow from baroclinic to barotropic components in the observed atmosphere with the FGGE data. When the waves reach finite amplitudes, the non-linear wave–wave interactions play the role to saturate the exponential growth. For this reason, the most unstable mode ξ_{1i} is anticipated to explain the largest fraction of the zonal–wave interactions.

2.4. *Construction of a barotropic model*

We now attempt in this study to construct a barotropic spectral model, using only the barotropic components (i.e., $m = 0$) of w_i for (14). The barotropic components capture the essential features of the low-frequency variability of planetary-scale motions. Such a model is equivalent to the predicting vertical average of meteorological variables. The spectral equation for such a barotropic model may have the same form as the baroclinic model of (4), except for an additional term of

barotropic–baroclinic interactions. When a barotropic subset is written for (14), linear terms retain the same form, but the non-linear wave–wave interactions are divided into interactions among barotropic components and those between barotropic and baroclinic components.

We assume first that the important energy supply to the barotropic component of the atmosphere is accomplished by the zonal–wave interactions represented by $a_l\xi_{li}$ rather than the wave–wave interactions of transient eddies. There are non-linear wave–wave interactions between barotropic and baroclinic components which may contribute to the barotropic–baroclinic interactions to some extent. However, those second order terms of transient eddies are considered of secondary importance in magnitude, compared with the dominant zonal–wave interactions. Second, the barotropic–baroclinic interactions are dominated by baroclinic instability associated with the most unstable mode $a_1\xi_{1i}$. All contributions from higher order eigenmodes are assumed to be less important due to the slow growth rates. With these assumptions, we attempt to close the system using only the barotropic components of w_i and ξ_{1i} for each zonal wavenumber as follows:

$$\frac{dw_i}{d\tau} + i\sigma_i w_i = -i\sum_{jk} r_{ijk} w_j w_k - i\nu_1 a_1 \xi_{1i} + f_i, \qquad i = 1, 2, 3, \ldots, L+1. \quad (15)$$

The 1st term of the right-hand side represents the non-linear wave–wave interactions among barotropic components of w_i. The second term in the right-hand side of (15) represents the wavemaker introduced in this study to amplify barotropic eddies in synoptic scale. It is a part of dynamical processes rather than an external forcing. Similar to the disregard numerous almost neutral eigenmodes, the term $i\sigma_i a_1 \xi_{1i}$ is also ignored since it is a neutral mode. Only the growing modes are considered to supply energy for the barotropic atmosphere. The barotropic model without the wavemaker is equivalent to the shallow water system. A similar barotropic model with the Hough mode expansion was successfully integrated first by Kasahara (1977) without the wavemaker. We have confirmed that the non-linear behavior of Rossby–Haurwitz wave as shown by Kasahara (1977) is successfully simulated with this model when the wavemaker is removed.

The amplitude coefficient $a_1(\tau)$ is supposed to be determined by solving a linear system (13) at every time step as mentioned before. It indicates a fraction of the state variables w_i explained by ξ_{1i}. Since we have assumed to employ only one eigenmode, it is reasonable to approximate it by an orthogonal projection of the state variable w_i onto the most unstable mode ξ_{1i}. It is known that the orthogonal projection tends to overestimate the fraction ξ_{1i} compared with solving a linear system since the eigenmodes are non-orthogonal. The orthogonal projection is supposed to be performed in the baroclinic atmosphere. However, the purpose of this study is not to integrate the baroclinic model (14), but to construct a barotropic model (15). There is no way to assume baroclinic components of w_i which is outside the model domain. Because the meaning of the amplitude coefficient a_1 is a fraction of the state variables w_i represented by ξ_{1i}, we performed the orthogonal projection within the barotropic atmosphere as follows:

$$w_i(\tau) = a_1(\tau)\xi_{1i} + \varepsilon_i(\tau), \quad (16)$$

where the vectors are reduced to include only the barotropic component, ξ_{1i} is normalized to have a unit norm $\sum_i \xi_{1i}^* \xi_{1i} = 1$, and $\varepsilon_i(\tau)$ is the orthogonal complement of the projection, i.e., $\sum_i \xi_{1i}^* \varepsilon_i = 0$. The amplitude coefficient $a_1(\tau)$ is thus evaluated every time step by a vector inner product for complex numbers:

$$a_1(\tau) = \sum_i \xi_{1i}^* w_i. \quad (17)$$

With the amplitude coefficient so obtained, the resulting wavemaker based on baroclinic instability is given as:

$$(BC)_i = -i\nu_1 a_1(\tau)\xi_{1i}. \quad (18)$$

The amplitude coefficient by (17) may overestimate the fraction ξ_{1i} compared with the case for the baroclinic atmosphere. When $a_1\xi_{1i}$ dominates the other eigenmodes in the baroclinic atmosphere as discussed in the linear framework, we can assume w_i is in proportion to $a_1\xi_{1i}$. For this special case, the amplitude coefficient by (17) evaluated in the barotropic atmosphere coincides with that evaluated in the baroclinic atmosphere. However, in general, w_i is not proportional to $a_1\xi_{1i}$, and not every fraction so projected may be associated with the baroclinic instability. An assessment for the performance of the present

wavemaker is conducted in reference to the result with the non-linear baroclinic model.

Fig. 4a schematically illustrates an evolution of the solution trajectory W for the non-linear system (4) in multi-dimensional phase space. The trajectory moves chaotically around the origin. When the system is linearized with respect to a zonal basic state as in (5) and small perturbations are superimposed on it, the trajectories of the small perturbations would behave as in Fig. 4b. Here,

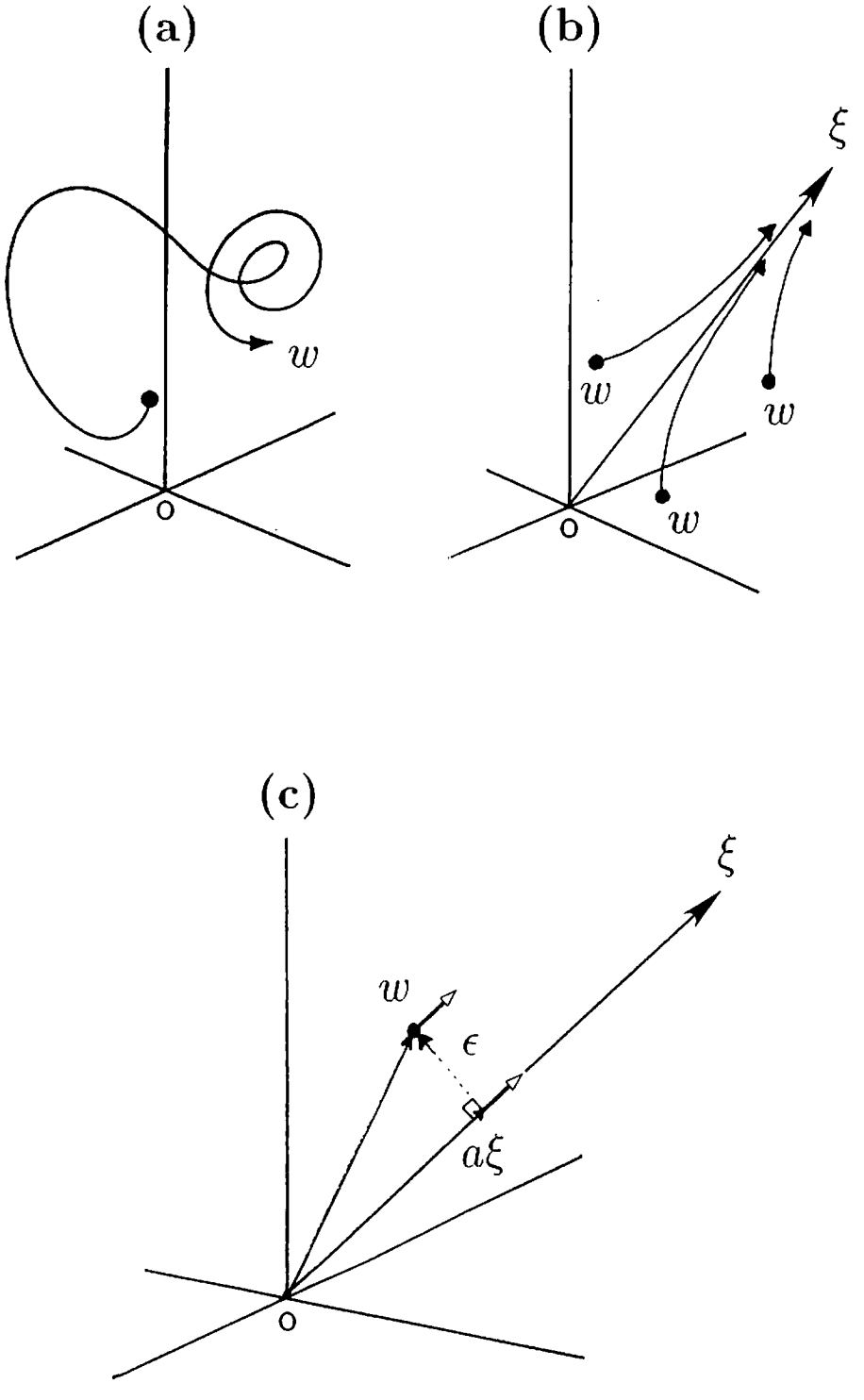

Fig. 4. Schematic illustration of a time evolution of the solution trajectory W in a phase space (a) for the nonlinear system (4); (b) for the unstable linear system (6); and (c) for the orthogonal projection of W onto the unstable direction ξ (16).

the trajectories starting at random initial points approach eventually to the most unstable direction ξ_1 and grows along the vector ξ_1 at the speed of the given growth rate. The situation and behavior in Figs. 4a, b should be the same even if we consider only the barotropic subset of W and ξ_1. Namely, the trajectory of the barotropic component of W approaches to the barotropic component of ξ_1 and grows along the vector ξ_1 at a given growth rate as in Fig. 4b. The amplitude factor $a_1(\tau)$ is determined by the orthogonal projection (16) and (17) as in Fig. 4c at every time step. The orthogonal projection is a reasonable representation of the exponential growth of the linear baroclinic instability as long as the non-linear term is negligible. A structure expected from baroclinic instability emerges from the infinitesimal white noise. Therefore, the parameterization (18) accurately traces the exponential growth of the vertical mean structure of baroclinic instability within the linear framework.

The linear theory no longer holds when the non-linear term becomes comparable to the forcing term by the baroclinic instability. The eddy growth would be reduced when the solution trajectory deviates from the unstable subspace $a_1\xi_1$. In practice, the baroclinic growth would completely vanish when the solution trajectory W becomes orthogonal to $a_1\xi_1$ due to the non-linear effect. As will be shown in the results, the exponential growth of the small perturbation eventually saturates when the non-linear wave–wave interactions begin to play the rôle. The energy supply due to the instability appears to balance with non-linear scattering toward the different scales. The performance of the present wavemaker at such a finite amplitude is the subject to be pursued in the future study.

2.5. *External forcing and energetics*

In this study, we consider only the following four physical processes as an external forcing:

$$f_i = (TF)_i + (DF)_i + (DZ)_i + (DE)_i, \tag{19}$$

where $(TF)_i$ represents the topographic forcing, $(DF)_i$ the biharmonic diffusion, $(DZ)_i$ the zonal surface stress, and $(DE)_i$ the Ekman pumping for eddies. Apart from the energy source of the topographic forcing, the sole energy source of the model is $(BC)_i$ induced by the baroclinic instability. The rest of the three physical processes are the energy sinks of the model. Refer to Tanaka (1998) for more comprehensive description of these forcings.

In the model, the total energy (i.e., the sum of kinetic energy and available potential energy) is monitored as one of the fundamental variables representing the global state of the atmosphere. In the spectral domain, the total energy is simply the sum of the energy elements E_i, which is defined by the squared magnitude of the state variable w_i:

$$E_i = \frac{1}{2} p_s h_m |w_i|^2, \tag{20}$$

where the subscript m is zero. By differentiating it with respect to time and substituting (15), we obtain the energy balance equation:

$$\frac{dE_i}{dt} = NL_i + BI_i + TF_i + DF_i + DZ_i + DE_i. \tag{21}$$

We use similar symbols as in (18) and (19), but without the parentheses for real-valued energy variables of dynamical and physical processes. The non-linear wave–wave interaction is designated by NL_i. Note that the linear term in the left-hand side of (15) does not contribute to the energy balance equation.

3. Results of the experiments

3.1. *Control run*

The model equation (15) is integrated in time, starting from an infinitesimal white noise superimposed on a zonal flow. In order to isolate the exponential amplification of unstable modes, the baroclinic instability is imposed in this study only at the zonal wavenumber 6. Fig. 5 illustrates the time evolution of the total energy for the zonal wavenumber 6 and the zonal motions. The energy level of the initial white noise superimposed on a zonal flow is of the order of 10 J m^{-2}. The energy level decreases for the first 20 days to 2 J m^{-2} due to the frictional dissipation. The energy level then starts to increase exponentially for days from 25 to 50 as expected from the linear theory. We can infer that the solution trajectory W is in parallel with ξ_1 as discussed in Fig. 4b. The exponential growth, however, must terminate when the wave amplitude becomes finite so that the non-linear wave–wave interactions become comparable to

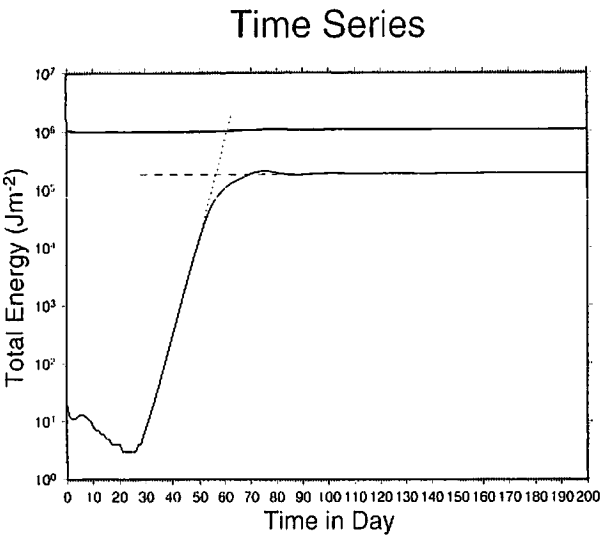

Fig. 5. Time series of total energy in the zonal (thick solid line) and eddy (thin solid line) components during the first 200 days. The crossing of dotted and dashed line represents the saturation point.

the linear terms in (15). This may be the stage of wave saturation. The eddy energy is equilibrated at 2×10^5 J m^{-2}. According to observation (Tanaka, 1985), the corresponding mean value for $n = 6$ is 3×10^4 J m^{-2}, i.e., about 10× smaller than the saturation level here.

By drawing two lines from the equilibrium level (dashed) and the exponential growth (dotted), we can determine the date of the wave saturation as day 55 in this example. Accordingly, the growth rate may be evaluated as 0.20 day^{-1} from the fact of increase by 5 orders of magnitude during 30 days in energy level. Since the growth rate for $n = 6$ is given as 0.34 day^{-1} by the linear stability analysis, we found that an appreciable fraction of growth rate was lost by the viscosity and frictional damping. Therefore, planetary waves of $n = 1$ to 4 may be hardly amplified by the linear instability alone since the growth rate is too small. The zonal barotropic energy is approximately constant at 1×10^6 J m^{-2}. It is interesting to note that the eddy energy reaches its equilibrium when the energy level becomes 20% of the zonal barotropic energy.

Fig. 6 illustrates hemispheric distributions of shallow water potential vorticity (PV) for days 48, 50, 52, 54, 100, 101, 102, and 200. A rotating wavenumber 6 emerges from infinitesimal noise in mid- to high-latitudes. When the wave amplitude is sufficiently small as for day 48, the structure is similar to the vertical mean of unstable Charney mode anticipated from baroclinic instability. Trough axis tilts from northwest to southeast at the northern flank of the Charney mode near 45°N, whereas it tilts from southwest to northeast at the southern flank of the Charney mode. The eddy momentum flux, thus, converges to mid-latitudes accelerating the westerly jet. When the amplitude becomes large enough as for day 54, high PV in the Arctic spreads away to lower latitudes maintaining the trough axis from northwest to southeast. At the same time, low PV in lower latitudes intrudes toward the Arctic. A positive and negative vorticity pair appears to rotate anti-clockwise at each sector. This is the time when wave saturation takes place according to the result in Fig. 5. The wave is about to break down, indicating a characteristic "surf zone" shape as shown in Fig. 3. Evidently, the meridional gradient of potential vorticity indicates negative area at the surf zone latitudes. The existence of the negative PV gradient is the necessary condition for the pattern to be unstable (see Charney and Stern, 1962; Garcia, 1991). Such an area appears on day 48 when the exponential growth of the unstable mode deviates from the theoretical straight line in Fig. 5.

However, it is interesting to note that the wave breaking has not occurred in this experiment as seen from PV distributions for days 100, 101, and 102. The surf zone shape of PV distributions attains a steady configuration, and it advects simply from west to east as is confirmed from the map of day 200. Although the meridional PV gradient is negative at some locations, the surf zone shape is stabilized in present model without developing into the wave breaking. Since the wave amplitude has saturated by definition as demonstrated in Fig. 5, the result of this study suggests that there is a case of equilibrium in the model atmosphere where the energy supply into the system balances with small frictional damping of harmonic waves.

Fig. 7 illustrates longitude–time section of potential vorticity along 58°N for this control run of the wave-6 experiment. Regular Rossby waves of wavenumber 6 are amplified by the parameterized baroclinic instability. The waves travel eastward and saturate the amplitudes around day 55. Then, the travelling waves maintain their amplitudes after the saturation. The eastward phase speed is approximately 12.4° day^{-1}. The regular movement of the

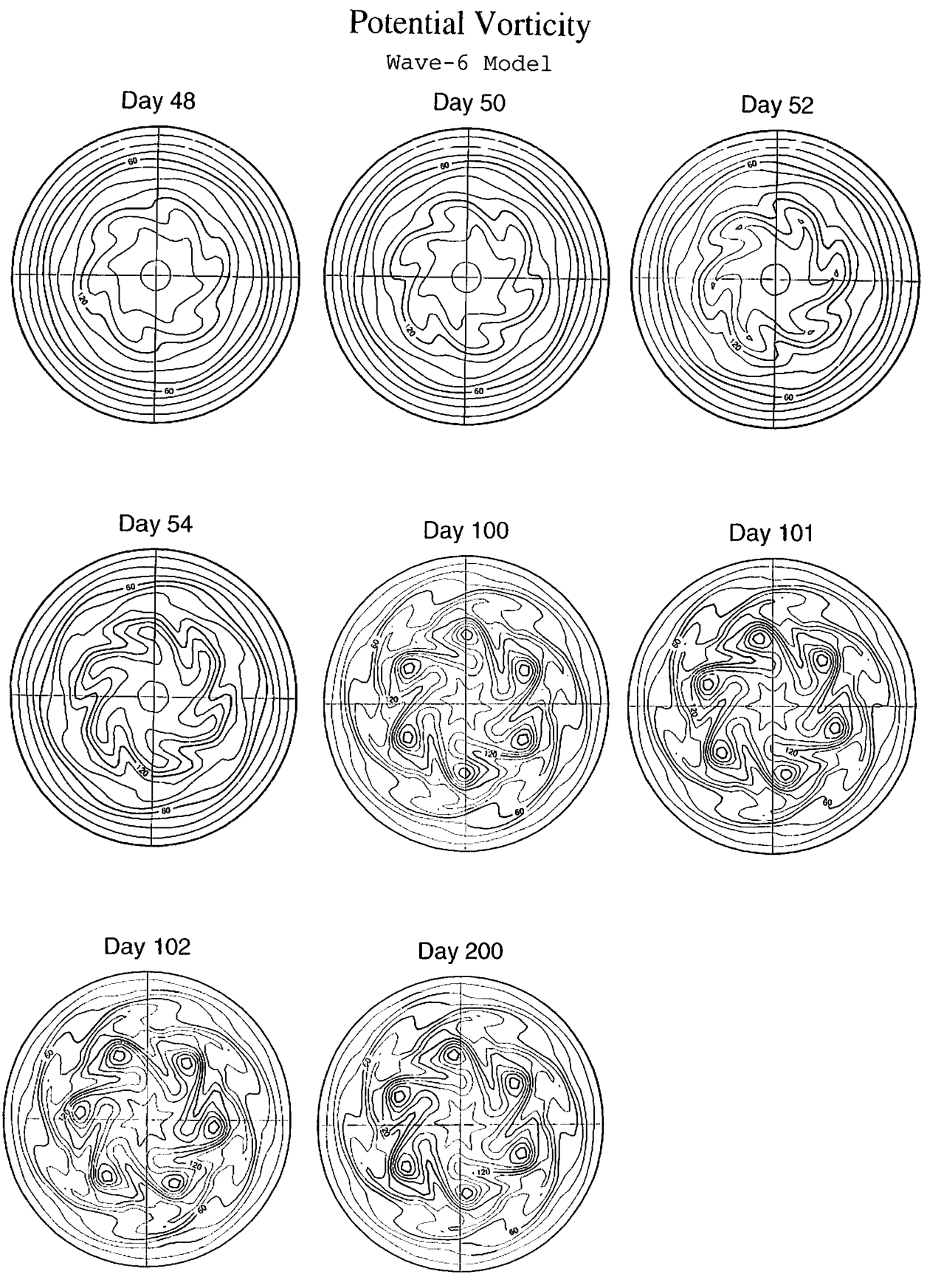

Fig. 6. Hemispherical distributions of potential vorticity with the wave-6 model for model days on 48, 50, 52, 54, 100, 101, 102, and 200. The units are $10^{-10}\,m^{-1}\,s^{-1}$ with the contour interval 15.

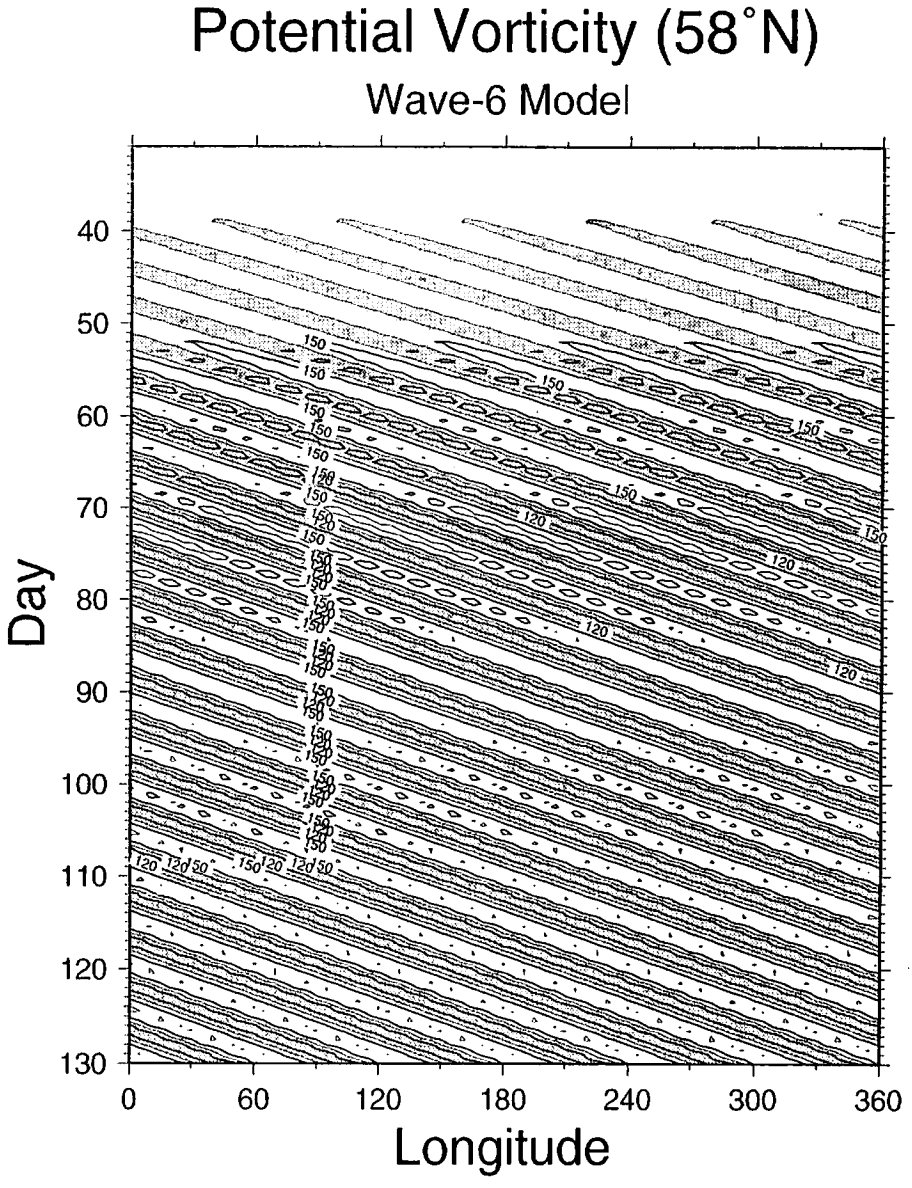

Fig. 7. Longitude–time section of potential vorticity along 58°N as in Fig. 2, but for the control run with the wave-6 model without topography during days 31 to 130.

wave-6 indicates the fact that the waves are saturating but not breaking. It may be possible, however, that the wave breaks down for a higher resolution model due to a small-scale instability. This equilibrium may be an artifact of the fixed shape of the parameterized baroclinic instability. We reserve it for the subject of the future study.

3.2. *Experimental run*

In this section of an experiment run, the regular travelling waves are intentionally destroyed by increasing the growth rate, Im(ν), until the waves break down. The first symptom of the Rossby wave breaking occurs when the growth rate is magnified by the factor 1.3. The same longitude–time section of potential vorticity as in Fig. 7, but with the magnification factor 1.3 is presented in Fig. 8. Here, we start the time integration from larger white noise than in Fig. 5 to save the computational time. The wave-6 is amplified quickly by baroclinic instability and is saturated around day 30. This time, the regularity in the phase speed is lost at day 50. Simultaneously, the wave amplitude is reduced substantially. Compared with the result in Fig. 7, we define this irregularity in the phase speed as a signal of Rossby wave breaking. The characteristics are

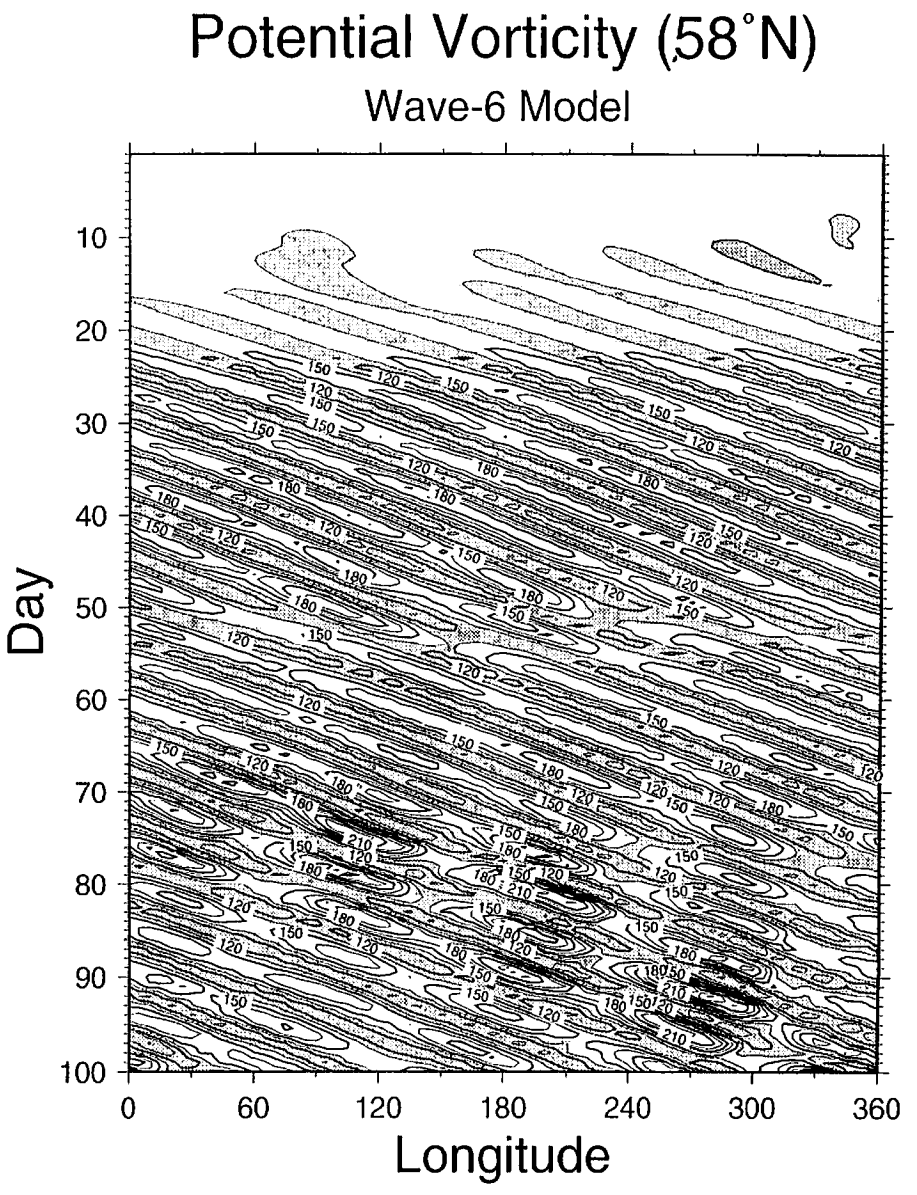

Fig. 8. As in Fig. 7, but for the experiment run with 1.3 times the growth rate during the first 100 days.

consistent with the breaking Rossby wave discussed in Fig. 2 in relation to the onset of blocking in the model atmosphere. The travelling wave-6 once recovers the regular progression around day 60. Yet, the wave breaking takes place repeatedly after day 80 indicating larger amplitudes and irregular phase speed.

Fig. 9 shows the hemispheric distributions of PV as in Fig. 6, but for the growth rate magnification factor 1.3 for days 49 to 52 when the Rossby wave undergoes breaking. For this experiment, the six cores of PV peaks in high latitudes exhibit different configurations, so it is realized that the sectorial symmetry of PV is now lost. Some well developed vortices undergo overturning of high and low PV distributions. Therefore, the wave breaking is characterized by the loss of sectorial symmetry and the overturning of the high and low PV distributions.

Fig. 10 illustrates the breaking Rossby waves expressed by the collection of 120 PV unit contours as functions of longitude and time for days 11 to 60. The wave amplitudes increase as time progresses, and the meridional gradient of PV turns to be negative around day 20. The surf zone shapes develop around day 25, but the waves keep moving forward preserving the surf zone shapes. The deformation of the 120 PV unit contours increases for days 40 to 50; this is the period when the wave breaking is identified. Some contours are

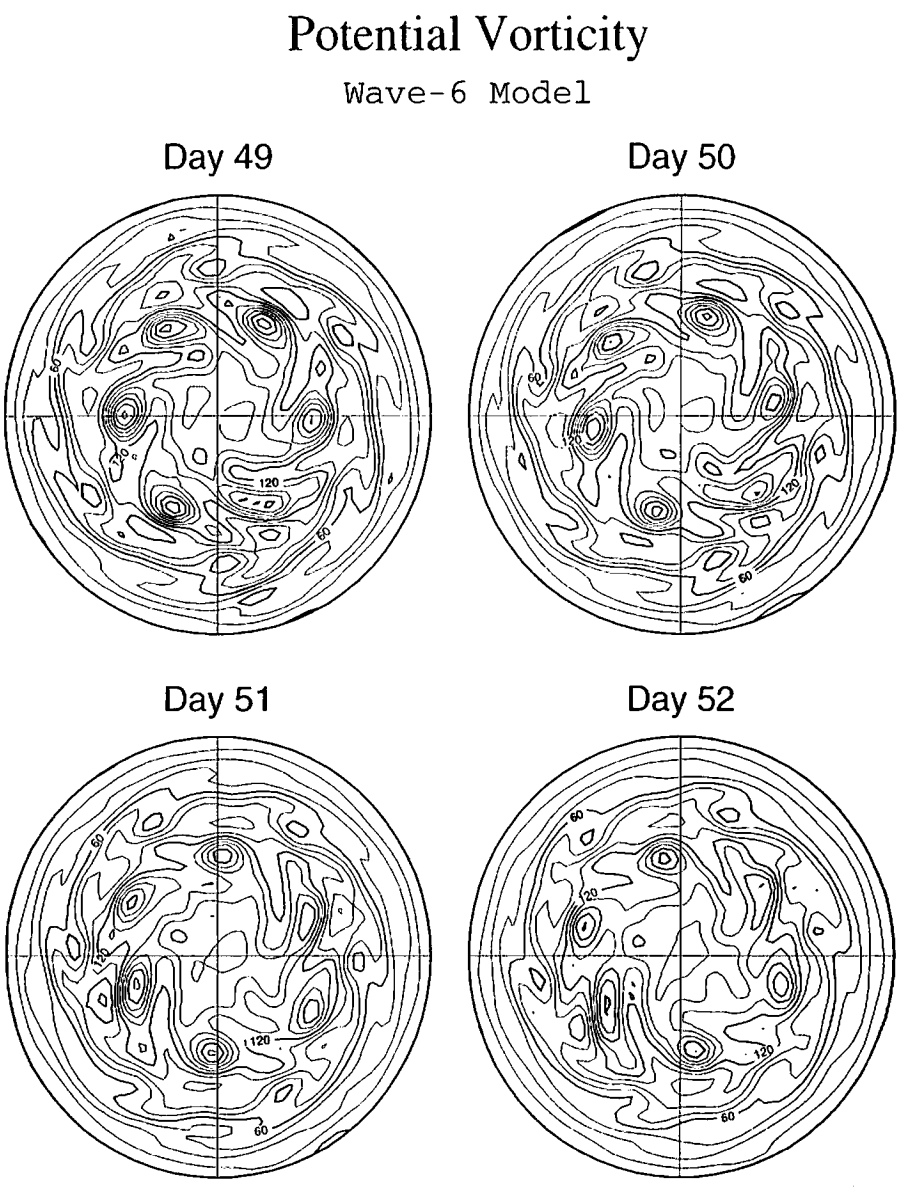

Fig. 9. As in Fig. 6, but for the experiment run with 1.3 times the growth rate for days 49 through 52 when the first wave-breaking occurs.

disconnected to produce a filament of PV contours. The wave amplitudes then gradually decrease for days 50 to 60.

The wave-6 experiment is repeated now with doubled growth rate to examine the wave breaking in an exaggerated situation. Fig. 11 is the same longitude–time section as Figs. 7, 8, but with the magnification factor 2.0 for the growth rate. The wave-6 amplifies quickly and attains a saturation point around day 25. The wave progression slows down after the saturation and irregularity begins after day 35. By the day 50, the dominant wavenumber is no longer 6, and the flow appears to be rather chaotic. The hemispheric distributions of PV for the doubled growth rate experiment are presented in Fig. 12 for days 53 to 56. Isolated coherent vortices are located irregularly within the domain. The number of cyclonic vortices may be counted as 6 for day 53, but it is no longer 6 by day 56 due to the vortex merging. The pattern may be recognized as very much turbulence.

3.3. Energetics analysis

Fig. 13 plots mean energy spectra over the zonal wavenumber domain for the wave-6 experiment during days 30 to 100 with various magnification factors for the growth rate. For the control run

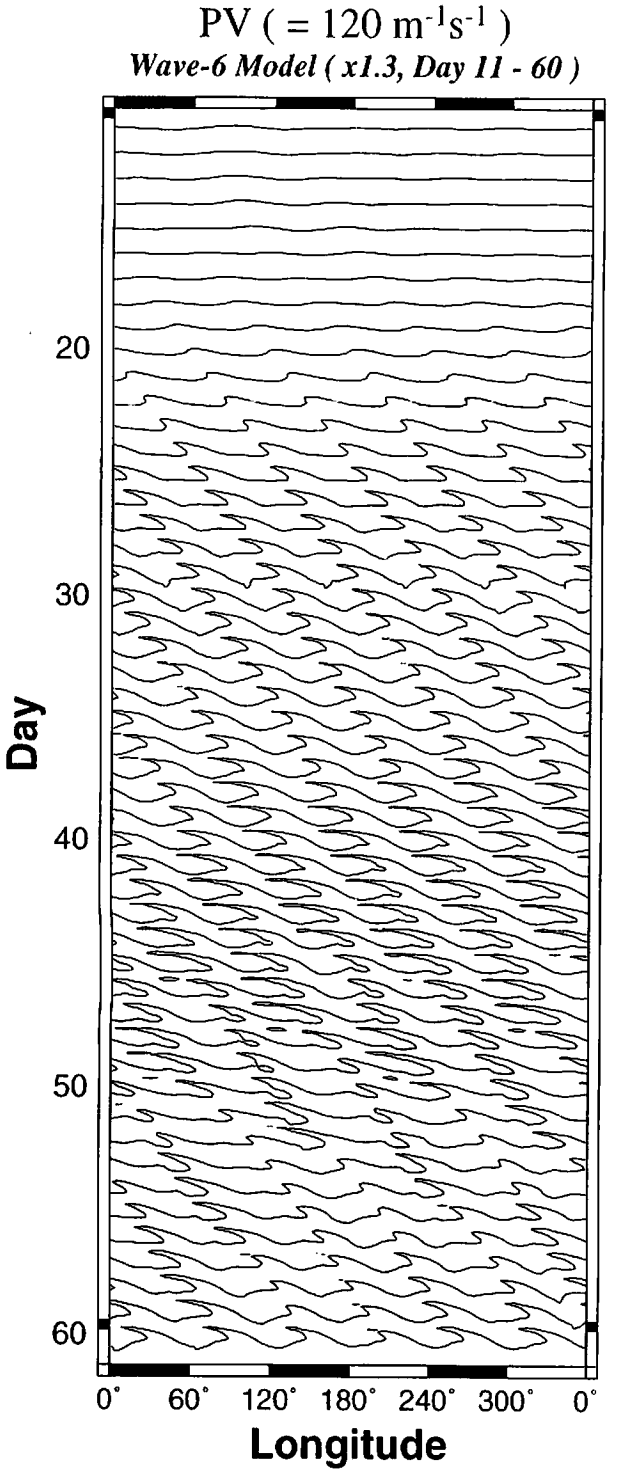

Fig. 10. Schematic illustration of breaking Rossby waves expressed by the contours of 120 PV in Fig. 9 as functions of time (day) and longitude.

with the magnification factor 1.0, the energy spectrum indicates sharp spectral peaks at $n = 6$, 12, and 18. Because of the amplified wave-6, its harmonics of $n = 12$ and 18 are excited through the weak non-linear interactions. As shown in Fig. 6 the control run maintains the steady configuration of the surf zone structure by the combination of those harmonic waves. The background noise energy in this case is of the order 10^2 J m^{-2}. When the growth rate is magnified by a factor 1.3, the three spectral peaks at $n = 6$, 12, and 18 remain recognizable. However, the main difference is seen in the high noise level at the rest of wavenumbers. The background noise in this case is enhanced by the strong non-linear wave–wave interactions reaching the order of 10^4 J m^{-2}. When the growth rate is doubled, the noise level becomes comparable to the spectral peaks. The spectral peaks at $n = 12$ and 18 are almost filled with the background noise. A result for the magnification factor 5.0 is plotted by a thick line. The spectral peak at $n = 6$ is recognizable, but its harmonics at $n = 12$ and 18 are completely lost in this case. More energy is accumulated in planetary waves than in $n = 6$, especially at $n = 1$ by means of the inverse energy cascade of the 2-D turbulence. The flow pattern (not shown) is strongly chaotic. It is interesting to note that the energy levels of the spectral peaks at $n = 6$ and its harmonics remain at the approximately same energy level despite the increased background noise level by the increased magnification factors for the growth rates.

Since the energy source is imposed only at $n = 6$ for this model, its harmonics and also the background noise must be excited by the unstable wave through the weak and strong non-linear wave–wave interactions, respectively. In Table 1, the energy flow within the zonal spectral domain is analyzed following the energetics scheme for the 3-D spectral model by Tanaka (1991). For the control run (Table 1a), energy is concentrated only at $n = 0$, 6, 12, and 18. The unique energy input of 0.973 W m^{-2} at $n = 6$ is dissipated by the amount of 0.288 W m^{-2} due to surface friction and eddy viscosity. The rest of 0.654 W m^{-2} is redistributed mostly to zonal flow by 0.595 W m^{-2} and to its harmonics of $n = 12$ and 18 by 0.046 and 0.012 W m^{-2}, respectively. The steady configuration of travelling Rossby waves presented in Fig. 6 is maintained by the energy balance listed in Table 1a. For the experiment run with the magnification factor 1.3, the wave–wave interactions redistribute the energy at $n = 6$ to all waves when Rossby waves break down for days 52 to 62 (Table 1b). For days 80 to 100 (Table 1c) the non-linear energy interactions become more active due

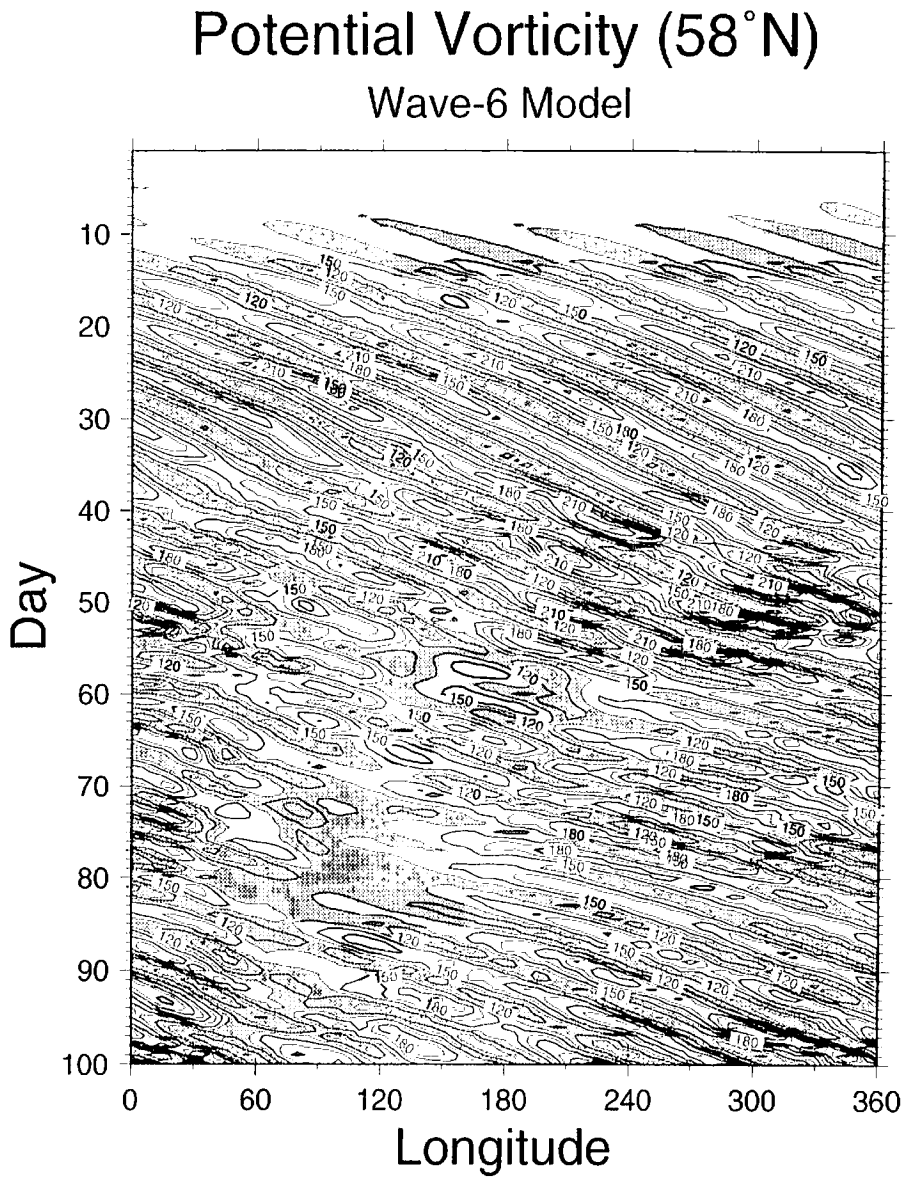

Fig. 11. As in Fig. 7, but for the experiment run with the doubled growth rate.

to the repeated Rossby wave breaking. Since energy has been accumulated in all waves, strong non-linear interactions can draw the energy from $n = 6$ and dissipate it effectively.

Finally, time series of zonal energy, unstable wave energy, and noise energy are presented in Fig. 14 for the control run and the experiment run with the magnification factors 1.3 and 2.0. Here, the unstable wave energy (dashed line) is the sum of $n = 6$, 12, and 18, and the noise energy (dashed line) is defined as the sum of the remaining eddy energy. For the control run in Fig. 14a, unstable waves are selectively amplified from the white noise after day 20. While the unstable waves grow exponentially for days 20 to 30, the noise energy keeps decreasing monotonically during the analysis period. The eddy energy (thin solid line) reaches its saturation point around day 40 and maintain the constant level thereafter. The zonal energy (thick solid line) keeps approximately the same level during the growing and breaking stages of wave-6. This is a special case of wave saturation without proceeding to wave breaking.

When the growth rate is enhanced by the factor 1.3 as in Fig. 14b, unstable waves grow rapidly after day 15 and saturate by day 25. The important difference between this experiment run and the former control run is seen in the increasing noise energy after the wave saturation for days 25 to 50. Energy transfer from unstable waves to back-

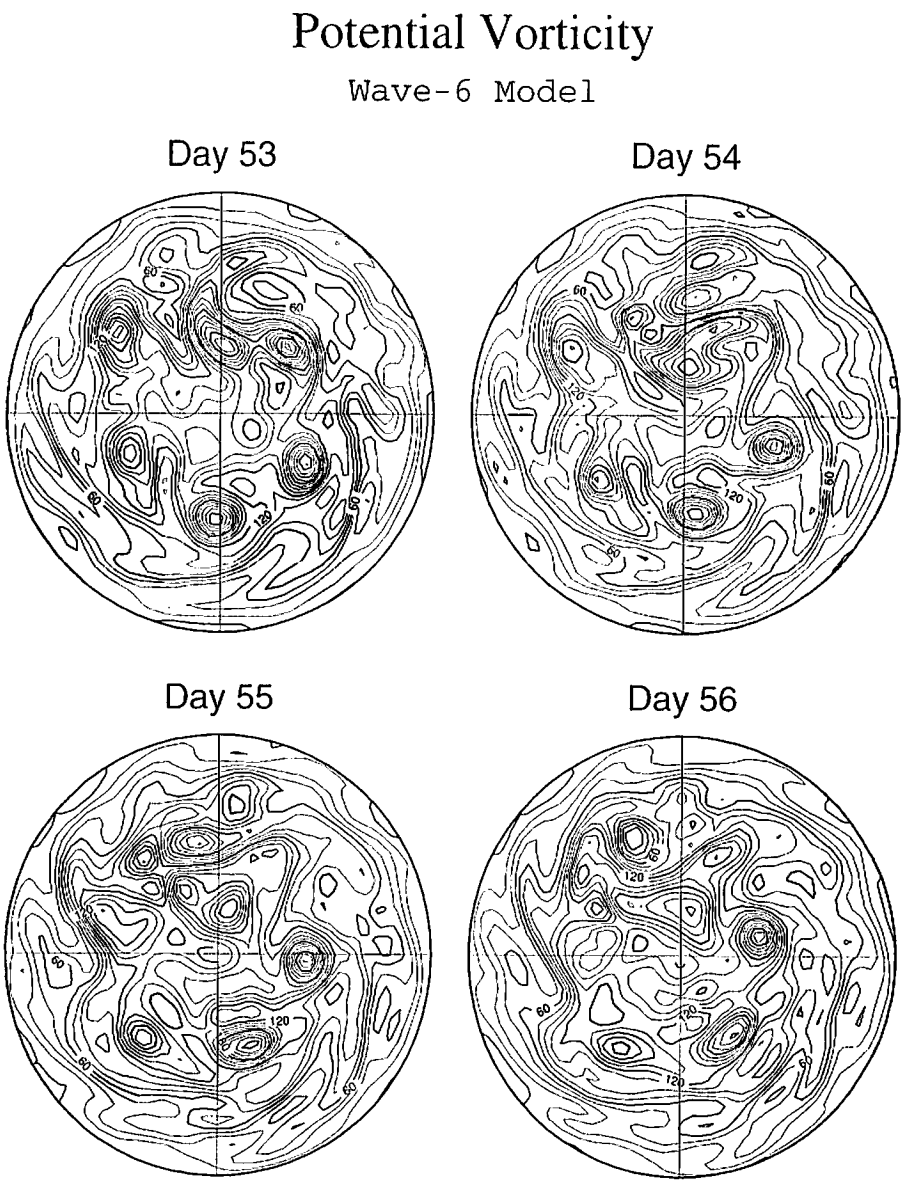

Fig. 12. As in Fig. 6, but for the experiment run with doubled growth rate for days 53 through 56.

ground noise is enhanced when the noise level becomes finite amplitude as inferred from the out-of-phase variation around day 50 between the two lines. When the noise energy level becomes comparable to the unstable wave energy, the unstable waves undergo wave breaking. The Rossby waves once recover the regularity around day 60 when noise level decreases as confirmed from Fig. 8. Yet, the flow pattern returns to the chaotic by the increased noise energy after day 80. The result for the doubled growth rate is presented in Fig. 14c. As in Fig. 14b the noise energy starts to increase after the unstable waves have saturated around day 15. Once the noise energy becomes comparable to the unstable wave energy, the flow appears to be chaotic owing to a sequence of wave breaking and vortex merging.

We consider the wave breaking as the realization of the increased background noise energy. It is suggested from the result that the energy supply by the dynamical instability must be large enough to excite the background noise for the criterion of the wave breaking.

Three different energy flow patterns are found associated with linear process, weakly non-linear process, and fully non-linear process. In the linear process, no wave–wave interactions, except for the zonal–wave interactions, are allowed. The energy supply must balance with dissipative damping of the given wave. In the weakly non-linear process,

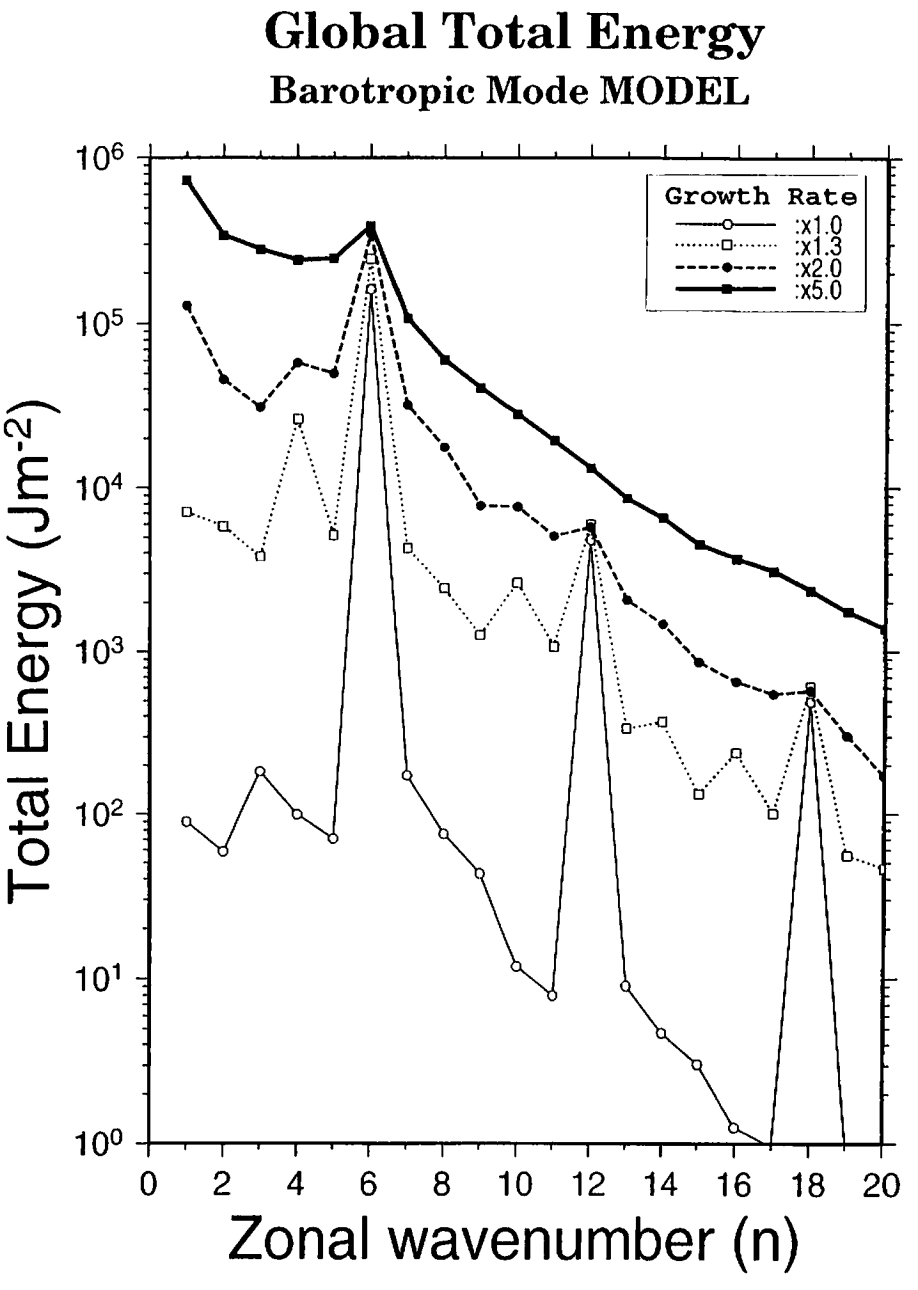

Fig. 13. Mean energy spectra over the zonal wavenumber domain for the wave-6 model during days 30 to 100 with various magnification for the growth rates.

harmonic waves in higher wavenumbers are allowed to amplify for a given unstable wave. The energy supply is then balanced with dissipation at all the harmonic waves. In the fully non-linear process, supplied energy can be transferred to all waves and balanced with the dissipative damping at all waves. The result of present study demonstrates the different class of equilibria, depending on the given energy supply controlled by the variable growth rate of the parameterized baroclinic instability. Since the weakly non-linear process has an upper bound in wave amplitudes due to the saturation, energy supply beyond the upper bound causes the excitation of the background noise energy. It is found in this study that the transition from weakly non-linear regime to fully non-linear regime in the energy transfer is the key factor for the Rossby wave breaking so that the supplied energy is effectively dissipated by all waves.

Table 1. *Time mean energy levels ($J\,m^{-2}$) and energy interactions ($10^{-3}\,W\,m^{-2}$) as functions of the zonal wavenumber n for (a) the control run of the wave-6 experiment for days 30–100, (b) the experiment run with 1.3 times the growth rate for days 52–62 and (c) that for days 80–100 (the symbol E represents energy level, BC baroclinic instability, NL non-linear wave–wave interaction, and DD the sum of diffusion and surface friction)*

	(a)				(b)				(c)			
n	$E(n)$	$BC(n)$	$NL(n)$	$DD(n)$	$E(n)$	$BC(n)$	$NL(n)$	$DD(n)$	$E(n)$	$BC(n)$	$NL(n)$	$DD(n)$
0	10748	0	595	−575	10705	0	644	−534	11031	0	771	−766
1	0	0	0	0	20	0	1	−3	176	0	33	−26
2	0	0	0	0	12	0	1	−2	140	0	26	−28
3	1	0	0	0	6	0	0	0	106	0	16	−17
4	0	0	0	0	79	0	−7	−11	629	0	79	−78
5	0	0	0	0	14	0	0	−2	143	0	34	−22
6	1616	973	−654	−288	1762	1329	−717	−304	2008	1505	−1122	−353
7	1	0	0	0	19	0	0	−2	80	0	18	−15
8	0	0	0	0	6	0	1	−1	56	0	19	−17
9	0	0	0	0	2	0	0	0	34	0	12	−10
10	0	0	0	0	9	0	1	−3	62	0	22	−21
11	0	0	0	0	2	0	1	−1	27	0	16	−12
12	49	0	46	−44	63	0	53	−49	34	0	27	−27
13	0	0	0	0	2	0	1	−1	6	0	5	−4
14	0	0	0	0	1	0	1	0	7	0	7	−5
15	0	0	0	0	0	0	0	0	3	0	4	−3
16	0	0	0	0	0	0	1	0	5	0	6	−6
17	0	0	0	0	0	0	0	0	2	0	4	−4
18	4	0	12	−11	6	0	14	−12	4	0	9	−7
19	0	0	0	0	0	0	0	0	1	0	2	−2
20	0	0	0	0	0	0	0	0	0	0	2	−1

4. Concluding remarks

In this study, we conducted a series of numerical experiments of breaking Rossby waves in the barotropic atmosphere using a simple barotropic model which implements parameterization of baroclinic instability. We examined the non-linear evolution of the finite amplitude Rossby waves in order to assess the criterion for the wave breaking. The baroclinic instability is imposed in this study only for zonal wavenumber 6 to isolate the process. Within the linear framework for small wave amplitudes, the parameterized baroclinic instability gives rise to a correct exponential growth of an unstable mode as expected from the linear theory. The expected structure of the most unstable mode emerges in the barotropic atmosphere from the infinitesimal white noise.

However, the exponential growth of the unstable waves must terminate ultimately when the wave amplitude becomes finite and the nonlinear wave–wave interactions become comparable to the linear terms. The energy supply for the growing waves is balanced with non-linear energy transfers to different waves. The phenomenon may be regarded as wave saturation. It is found in this study that the exponential growth of the unstable wave-6 is saturated when the wave energy reaches approximately 20% of zonal energy of the basic flow.

For the ordinary growth rate, we found a case such that the waves are saturating but not breaking. For a control run of the wave-6 experiment, the saturated waves travel eastward maintaining the steady configuration of surf zone shape. The appearance of the negative meridional gradient of PV is the necessary condition for the wave saturation according to Charney and Stern (1962) and Garcia (1991). Despite the fact of the apparent negative meridional gradient around the surf zone latitudes, the Rossby wave has not undergone the wave breaking. According to the energetics ana-

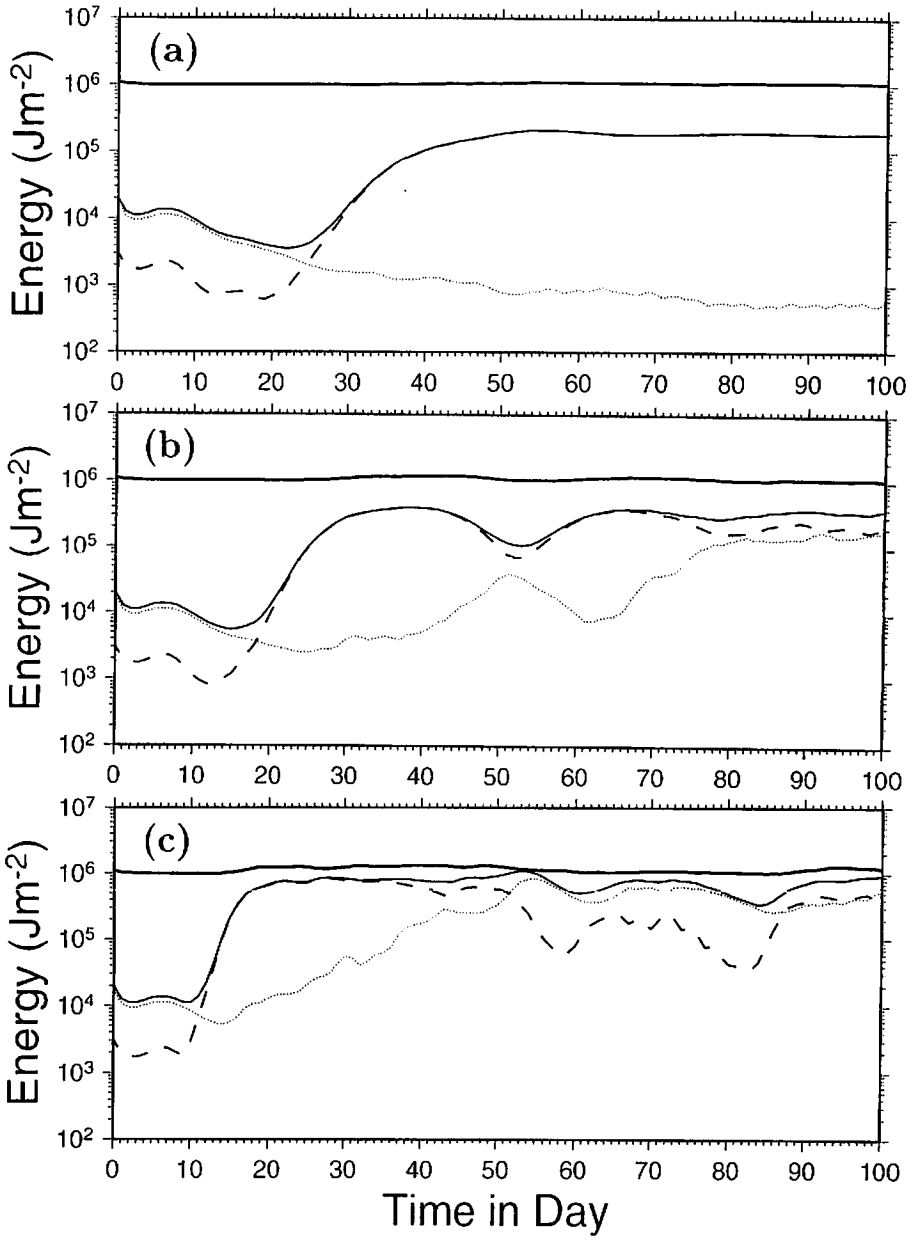

Fig. 14. Time series of total energy in the zonal (thick solid line) and eddy (thin solid line) components during the first 100 days. The eddy components are further divided in the sum of harmonic waves of $n = 6$, 12, and 18 (dashed line) and the rest of the non-harmonic waves (dotted line). (a) for the control run; (b) for the 1.3 times the growth rate; and (c) for the doubled-growth rate, respectively.

lysis, the energy supply at wave-6 is equilibrated with energy transfer to zonal motions and to its harmonics in higher wavenumbers. This is a special case of an equilibrium attained by the weakly non-linear energy transfers.

Next, we attempted to break the equilibrated waves artificially by increasing the growth rate of the unstable mode. It is found that the regularity of steady Rossby wave progression is lost and the overturning of high and low PV centers begins when the growth rate is increased by 30%. This phenomenon may be recognized as wave breaking. The overturning of the vortex pair is mostly anti-clockwise for present wave-6 model. The major difference compared with the control run is seen at the increased energy level of background noise through the fully non-linear interactions among all waves. Associated with the Rossby wave breaking, not only the harmonic waves but all zonal waves are amplified by the fully non-linear interactions among all waves. The Rossby wave breaking may be the realization of the increased

background noise energy. It is demonstrated in this study that the transition from the weakly non-linear regime to fully non-linear regime in the energy transfer is the key factor for the Rossby wave breaking so that the supplied energy is effectively dissipated by all waves.

Finally, we note that the result of this study is based on first 100-day simulations of a simple barotropic model with a rather coarse resolution. The result should be confirmed using a higher resolution model. The stable surf zone structure in the control run might be destabilized by small disturbances as demonstrated by Haynes (1989). The parameterization of baroclinic instability in this study is useful to excite required amount of synoptic eddies in a barotropic model. However, the detail of the non-linear evolution indicates some contradictions compared with previous studies with full baroclinic models (Simmons and Hoskins, 1976; Thorncroft et al., 1993; Whitaker and Snyder, 1993; Tanaka, 1995; Balasubramanian and Garner, 1997; Hartmann and Zuercher, 1998). Because the computational domain is restricted to the barotropic component of the atmosphere, baroclinic structure of the zonal field is assumed to be fixed. Therefore, there is no eddy feedback to the zonal baroclinicity. This assumption may be inappropriate for the correct parameterization for the life-cycle of baroclinic waves. However, present study is concerned only with the breaking Rossby waves in the barotropic atmosphere. In this regard, present parameterization of baroclinic instability may be referred to simply as a wavemaker, or baroclinic stirring. Further modifications of present wavemaker are desired for quantitative application of general circulation studies.

5. Acknowledgements

This research was supported by the Grant-in-Aid for Scientific Research, Japanese Ministry of Education, Science, Sport and Culture, no. 09640518. The authors appreciate Ms. K. Honda for her technical assistance.

REFERENCES

Akahori, K. and Yoden, S. 1996. Zonal flow vacillation and bimodality of baroclinic eddy life cycles in a simple global circulation model. *J. Atmos. Sci.* **54**, 2349–2361.

Balasubramanian, G. and Garner, S. T. 1997. The role of momentum fluxes in shaping the life cycle of a baroclinic wave. *J. Atmos. Sci.* **54**, 510–533.

Charney, J. G. and Stern, M. E. 1962. On the stability of internal baroclinic jet in a rotating atmosphere. *J. Atmos. Sci.* **19**, 159–172.

Fritts, D. C. 1984. Gravity wave saturation in the middle atmosphere. A review of theory and observation. *Rev. Geophys. Space Phys.* **22**, 275–308.

Garcia, R. R. 1991. Parameterization of planetary wave breaking in the middle atmosphere. *J. Atmos. Sci.* **38**, 2187–2197.

Govindasamy, B. and Garner, S. T. 1997. The equilibration of short baroclinic waves. *J. Atmos. Sci.* **54**, 2850–2871.

Hartmann, D. L. and Zuercher, P. 1998. Response of baroclinic life cycle to barotropic shear. *J. Atmos. Sci.* **42**, 865–883.

Haynes, P. H. 1989. The effect of barotropic instability on the nonlinear evolution of a Rossby wave critical layer. *J. Fluid Mech.* **207**, 231–266.

Juckes, M. N. 1989. A shallow water model of the winter stratosphere. *J. Atmos. Sci.* **46**, 2934–2955.

Juckes, M. N. and McIntyre, M. E. 1987. A high-resolution one-layer model of breaking planetary waves in the stratosphere. *Nature* **328**, 590–596.

Kasahara, A. 1977. Numerical integration of the global barotropic primitive equations with Hough harmonic expansions. *J. Atmos. Sci.* **34**, 687–701.

Lindzen, R. S. 1981. Turbulence and stress owing to gravity wave and tidal break down. *J. Geophys. Res.* **86**, 9707–9714.

Leovy, C. B., Sun, C.-R., Hitchman, M. H., Remsberg, E. E., Russell, J. M. III, Gordley, L. L., Gille, J. C. and Lyjak, L. V. 1985. Transport of ozone in the middle stratosphere: evidence for planetary wave breaking. *J. Atmos. Terr. Phys.* **42**, 230–244.

McIntyre, M. E. and Palmer, T. H. 1983. Breaking planetary waves in the stratosphere. *Nature* **305**, 593–600.

McIntyre, M. E. and Palmer, T. H. 1984. The 'surf zone' in the stratosphere. *J. Atmos. Terr. Phys.* **46**, 825–849.

McIntyre, M. E. and Palmer, T. H. 1985. A note on the general concept of wave breaking for Rossby and gravity waves. *Pure Appl. Geophys.* **123**, 964–975.

Robinson, W. A. 1988. Irreversible wave–mean flow interactions in a mechanistic model of the stratosphere. *J. Atmos. Sci.* **45**, 3413–3430.

Shutts, G. J. 1983. The propagation of eddies in diffluent jet streams: eddy vorticity forcing of blocking flow fields. *Quart. J. Roy. Meteor. Soc.* **109**, 737–761.

Simmons, A. J. and Hoskins, B. J. 1976. Baroclinic instability on the sphere: normal modes of the primitive and quasi-geostrophic equations. *J. Atmos. Sci.* **33**, 1454–1477.

Tanaka, H. L. 1985. Global energetics analysis by expansion into three-dimensional normal mode functions during the FGGE winter. *J. Meteor. Soc. Japan* **63**, 180–200.

Tanaka, H. L. 1991. A numerical simulation of amplification of low-frequency planetary waves and blocking formations by the upscale energy cascade. *Mon. Wea. Rev.* **119**, 2919–2935.

Tanaka, H. L. 1995. A life-cycle of nonlinear baroclinic waves represented by 3-D spectral model. *Tellus* **47A**, 697–704.

Tanaka, H. L. 1998. Numerical simulation of a life-cycle of atmospheric blocking and the analysis of potential vorticity using a simple barotropic model. *J. Meteor. Soc. Japan* **76**, 983–1008.

Tanaka, H. L. and Kung, E. C. 1989. A study of low-frequency unstable planetary waves in realistic zonal and zonally varying basic states. *Tellus* **41A**, 179–199.

Tanaka, H. L. and Sun, S. 1990. A study of baroclinic energy source for large-scale atmospheric normal modes. *J. Atmos. Sci.* **47**, 2674–2695.

Throncroft, C. D., Hoskins, B. J. and McIntyre, M. E. 1993. Two paradigms of baroclinic-wave life-cycle behavior. *Q. J. Roy. Meteor. Soc.* **119**, 17–55.

Whitaker, J. S. and Snyder, C. 1993. The effects of spherical geometry on the evolution of baroclinic waves. *J. Atmos. Sci.* **50**, 597–612.

Warn, T. and Warn, H. 1978. The evolution of a nonlinear critical level. *Stud. Appl. Math.* 359, 37–71.